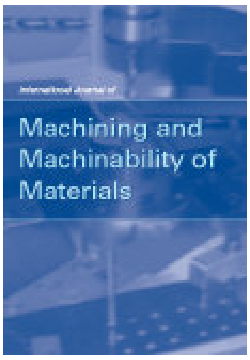

International Journal of Machining and Machinability of Materials

ISSN online: 1748-572X - ISSN print: 1748-5711
https://www.inderscience.com/ijmmm

Turning parameters optimisation for Inconel 800H under MQL environment based on Harris hawks optimisation algorithm coupled with TOPSIS method

H. Bharath, K. Venkatesan, S. Devendiran

DOI: 10.1504/IJMMM.2023.10053891

Article History:

Received:	12 August 2022
Last revised:	24 November 2022
Accepted:	23 December 2022
Published online:	15 March 2023

Turning parameters optimisation for Inconel 800H under MQL environment based on Harris hawks optimisation algorithm coupled with TOPSIS method

H. Bharath, K. Venkatesan* and S. Devendiran

School of Mechanical Engineering,
Vellore Institute of Technology,
Vellore, Tamil Nadu, India
Email: bharath.h@vit.ac.in
Email: venkatesan.kannan@vit.ac.in
Email: devendiran@vit.ac.in
*Corresponding author

Abstract: In this study, turning operations were performed to optimise the surface roughness, cutting force, and residual stress. Trials were done on Inconel 800H using olive oil mixed with 0.20 wt % hexagonal boron nitride. Response surface methodology has established a link between input and machining responses. Harris hawk optimisation (HHO) was used to search for potential candidates for the solution. A technique for order preference by similarity to the ideal solution (TOPSIS) was used to detect the most viable compromise. The optimal results of TOPSIS-HHO are benchmarked with other metaheuristic algorithms. The results show that the optimum results and their responses found through experiments are R_a 0.2837 μm, F_z 137 N, and Res 406 MPa, which are less than a 10% average error on the predicted value. The HHO-TOPSIS showed an improvement in convergence rate by 9.57%, 12.04%, 11.73%, and 32.65% at the optimal determined values compared to other hybrid algorithms.

Keywords: Inconel 800H; minimum quantity lubrication; MQL; tool wear; Harris hawk optimisation; HHO; analysis of variance; ANOVA; TOPSIS.

Reference to this paper should be made as follows: Bharath, H., Venkatesan, K. and Devendiran, S. (2023) 'Turning parameters optimisation for Inconel 800H under MQL environment based on Harris hawks optimisation algorithm coupled with TOPSIS method', *Int. J. Machining and Machinability of Materials*, Vol. 25, No. 1, pp.41–68.

Biographical notes: H. Bharath is currently doing his PhD degree in the School of Mechanical Engineering, Vellore Institute of Technology, Vellore, Tamilnadu, India. His current research interests are advanced manufacturing technologies, smart manufacturing, optimisation, and machining technologies of difficult-to-cut materials.

K. Venkatesan is an Associate Professor Senior in the School of Mechanical Engineering, Vellore Institute of Technology, Vellore, Tamilnadu, India. He received his PhD degree in Mechanical Engineering from Vellore Institute of Technology, Vellore, Tamilnadu, India. His industry, teaching, and research experience is 15 years. His research interests include laser assisted machining, micromachining, materials engineering machining technologies for difficult-to-cut materials optimisation, composites, smart manufacturing, and the application of artificial intelligence techniques.

S. Devendiran is a Professor in the School of Mechanical Engineering, Vellore Institute of Technology, Vellore, Tamilnadu, India. He received his PhD degree in Mechanical Engineering from Vellore Institute of Technology, Vellore, Tamilnadu, India. His industry, teaching, and research experience is 16 years. His research interests include machining technologies for difficult-to-cut materials, vibration, optimisation, smart manufacturing, and the application of artificial intelligence techniques.

1 Introduction

The superalloys are used in many industries, including automotive, nuclear, petroleum, space, and chemical, for their high strength. Nickel based superalloys are widely utilised in the aircraft industry; specifically, gas turbine engine utilisation was nearly 45–50% (Palanisamy and Selvaraj, 2018; Angappan et al., 2017). Inconel 800H, an iron-based superalloy, has a high withstand temperature of 810°C and is used in power, petrochemical, nuclear plants, and heat exchangers components. This alloy is used as a cutting tool in machining because of the material's high creep strength and higher oxidation-corrosion resistance capability. Inconel 800H is hard-to-machine material following important properties like rapid hardening, low thermal conductivity, and rapid tool work adhesion (Palanisamy et al., 2021; Byrne and Scholta, 1993). Machining such alloy in a dry condition is a comprehensive task and leads to poor machinability, damage to tools, and poor surface finish. To meet such challenges, minimum quantity lubrication (MQL) technology is applied and succeeded in many machining applications (Majak et al., 2020). In machining processes, 85% of cutting fluids are petroleum-based oils. In addition, non-toxic, non-negative impact, and ecologically sustainable cutting fluids are preferable over petroleum oils (Robinson Gnanadurai and Mesfin, 2022). Furthermore, tribological studies of vegetable oils demonstrated outstanding anti-friction and anti-wear capabilities. Other improvement includes biodegradability, ease of readiness, and affordability. In addition, many researchers applied vegetable oil such as coconut oil, olive oil, sunflower oil, canola oil, sesame oil, and other oils as cutting fluids in various machining applications. For example, Saleem and Mehmood (2022) investigated the performance of sunflower (MQLSO) and castor oil (MQLCO) during the turning of Inconel 718. The results showed that the MQLSO outperformed other MQLCO and dry because of sunflower properties (viscosity and ability to wet the surface better). The tool wear and surface roughness obtained with MQLSO improved better than the dry conditions. Singh et al. (2022) studied the performance of three oils, synthetic oil (SO: local brand), vegetable oil (VO: soybean oil), and used motor oil (UO: 10W-30), during the MQL turning of Hastelloy C-276. The experimental results revealed that VO improved roughness in MO compared to SO at the lower levels of input parameters. The SEM results reveal lower flank wear values during VO than SO. Rapeti et al. (2018) conducted an MQL-turning on AISI 1040 steel with coconut oil, sesame oil, and canola oil dispersed with MoS2. This study concluded that coconut oil nano-MQL (NMQL) is very capable and promising in machining to reduce surface roughness, cutting tool temperature, tooltip wear, and cutting force. Vasu and Pradeep Kumar Reddy (2011) accomplished a comparative turning process on Inconel 600 using three lubrication methods (dry, MQL, and NMQL). The results concluded that the NMQL lubrication technique attained reduced force, temperature, roughness, and flank wear. Jeevan and Jayaram (2018) examined the performance of Jatropha, Pongamia, and mineral oils as MQL in turning AA6061, where noticeable lower flank wear and reduced cutting force were observed during Pongamia oil in MQL machining. Talib et al. (2017) investigated and compared the tribological performance of different concentrations of hexagon boron nitride (hBN) with modified jatropha oil to crude jatropha oil and synthetic ester (SE). Modified jatropha oil with lower hBN exhibited better friction and wear behaviour reduction with superior machining performance than other tested oil. The study also reported lesser weight percent of hBN particles in altered oil significantly reduced the cutting force, temperature, and tool chip contact length and improved surface quality and tool life. Hegab et al. (2018) reported the performance of multiwall carbon nanotube (MWCNT) and Al_2O_3 with rapeseed oil MQL lubricant method in turning Inconel 718, where MWCNTs with rapeseed oil MQL outperform Al_2O_3 and given significant changes in modes of tool wear. Yıldırım et al. (2019) investigated the process performance of tool life, surface roughness, and temperature of Inconel 625 in four different cutting environments: dry, pure MQL (plantocut 10 SE), MQL machining with 0.5 vol.% hBN and MQL machining with 1.0vol%hBN. MQL with 0.50 vol.% hBN produced excellent surface finish, lower tool wear, and high tool life. Korkmaz et al. (2021) studied the performance of duple-jets MQL and hBN nanoparticles (1.0 wt.%) with WerteMist on turning of Nimonic 80A. The study reveals that the position of the nozzle plays an important role in the machining improvement during the turning of alloy. The hBN nanofluids showed an improvement in tool wear compared to dry. Abrasion and adhesion are two major tool wear mechanisms observed in dry. Venkatesan et al. (2020) investigated the application of hBN particles with a range of weight percentages blended with groundnut oil as nanofluid on turning of Nimonic 90 alloy and found the improved surface roughness and cutting force in comparison to dry condition. Huang et al. (2018) effectively studied the influence of electrostatic minimum quantity lubricant (EMQL) on cutting force, roughness, and tool wear during turning AISI 304 stainless steel and compared it with dry, conventional wet, and MQL. The oil mist input parameters are charging voltage, lubricant flow rate, nozzle angle, distance, and air pressure. Results found that surface roughness and cutting force decreased with the fluid flow rate increase. On the other hand, the force decreases, but roughness increases when air pressure increases. Liu et al. (2011) studied the effect of air pressure, oil flow rate, and nozzle position in MQL-based end-milling Ti-6Al-4V. The oil flow rate was vital in decreasing cutting force and temperature. Therefore, a well-chosen set of MQL parameters is required for a highly proficient MQL system. Ross et al. (2022a) studied the effect of the hybrid cooling approach during the machining of Nimonic 80A and compared it with MQL and cryogenic conditions. The results revealed that the hybrid C/L decreased temperature and specific consumption energy compared to MQL. Singh and Sharma (2022) studied the effect of different lubrication strategies (dry, flood, UAF) during the machining of Hastelloy C-276. The results showed a reduction in cutting force, feed force, radial force, and roughness under UAF compared to dry and flood. Zhou et al. (2022) studied the effect of dry, MQL, and cryogenic conditions on the force, roughness, temperature, and tool wear during the turning of Hastelloy-X. Cutting forces were reduced with MQL and cryogenic cooling compared to dry conditions. The measured surface roughness values are lowest under the cryogenic cooling condition. The adhesion and chipping wear mechanism observed on the tool edge was reduced with cryogenic cooling. Sun et al. (2022) studied the influence of different lubrication strategies (dry, MQL (pure oil), and pure oil mixed with water) on the cutting performance of high-speed machining of GH4099. The results reveal a reduction in milling force for MQL and MQL mixed with water compared to dry milling. The cutting temperature was reduced significantly for the above two lubrication strategies. In addition, improving the workpiece's surface quality was observed under MQL and water+pure oil. Compared to dry milling, adhesive wear, diffusion wear, and notch wear are the dominant tool wear mechanisms under MQL and water+Pure oil. Ross et al. (2022a) studied the effect of different cooling and lubrication environments on Monel-400 alloy. The study's results highlighted that flank wear reduction was observed under CO_2 + MQL compared to dry, MQL, and CO_2 conditions.

Different optimisation approaches have been used in the literature to optimise the process parameters due to the effective MQL C/L. For example, Gupta and Sood (2017) reported that particle swarm optimisation (PSO) and bacterial foraging optimisation (BFO) performed better in optimising the machining parameters on cutting force, tool wear, chip control, and roughness than the desirability function approach of Inconel 800 under MQL environment. Rubaiee et al. (2022) reported that non-dominated sorting genetic algorithm II (NSGA-II) and the teaching-learning-based optimisation (TLBO) approach) to determine the same optimal combination of machining indices turning of Inconel 718 under four lubrication mediums (dry, MQL, nMQL, and cryogenic). Sivalingam et al. (2021) reported that the Moth-Flame optimisation (MFO) algorithm outperformed compared to genetic (GA), Grass-Hooper (GH), grey-wolf (GW), and PSO algorithms in finding the range of reduction in force, roughness, and cutting temperature values in turning Hastelloy X. Salem et al. (2021) evaluated an experimental study on Inconel 718 using both nano additives (MCNT and Al_2O_3), and NSGA-II was applied for muli-objective optimisation. It was found that the Al_2O_3 Nanofluid shows better performance for the machining cost. In comparison, the MCNT nanofluid shows better performance for energy. Elsheikh et al. (2021) applied hybrid models composed of a conventional ANN model (C-ANN) combined with two bioinspired optimisers, such as the pigeon optimisation algorithm (POA) and PSO, to predict residual stresses during the machining of Inconel 718. Compared to C-ANN, both hybrid machining learning (ML) models showed good prediction accuracy for residual stress. Further, POA is suggested to improve the prediction accuracy of the conventional ANN. Viswanathan et al. (2020) used a combination of Grey relation and principal component analysis to find the optimal process parameters. It was reported that the cutting depth influences and dominates much on desired surface roughness and cutting force on AZ91D Magnesium alloy. Han et al. (2020) developed a multi-objective model to determine the trade-off between cutting power (P) and material removal rate (MRR) in the milling process. GRA was used to determine the weight of the objective functions. Linear Decreasing Particle Swarm Algorithm (LDPS) optimisation algorithm optimised the cutting parameters for producing maximum MRR while minimising cutting power. Hegab et al. (2021) developed an evolutionary optimisation algorithm based on soft computing intelligent methods for the MQL turning of Inconel 718. The modelling of the machining process (tool wear, surface quality, and energy consumption) developed using soft computing methods of ANN, adaptive neuro-fuzzy inference system (ANFIS), and genetic programming (GP) was compared with RSM models. In addition, a non-dominated sorting genetic algorithm (NSGA-II) optimised the process parameters. The GP models achieved the highest determination coefficient in predicting the process variables compared with other soft-computing methods. Abbasi et al. (2021) used the Harris hawk optimisation (HHO) method for microchannel heat sinks. To minimise the formation of entropy, it stated that the exploitation and exploration capability of the HHO results are better when compared with the whale optimisation algorithm, dragonfly algorithm, bees optimisation algorithm, PSO, and grasshopper optimisation algorithm.

The literature shows that MQL, MQL, NMQL, and cryogenic are promising and viable substitutes for machining performance improvement during nickel-based super alloys compared to dry and flood. However, further improvement in performance indicators, MQL (oil-mist), and machining parameters must be optimised together for multiple purposes with advanced algorithms. Hitherto, no mathematical model has been determined using RSM, which can predict MQL and machining parameters on output responses in turning nickel based alloy. By considering all the facts taken into account, the current study has two objectives. First, to study the effect of MQL (oil mist) parameters on machining performance. Second, use contemporary methods to improve machining characteristics by optimising the combined MQL and cutting parameters. In this context, the presented research work is focused on using the recent swarm-based intelligence algorithm, so-called HHO, coupled with technique for order preference by similarity to the ideal solution (TOPSIS) to obtain the most optimal feasible solution. Finally, design variables (optimal parameters) and their attainment have been compared to the results of the various benchmarked algorithms.

2 Materials and methods

Inconel 800H was the workpiece material used in this study for conducting experiments. It measures 32 mm in diameter × 300 mm in length. The experiments were conducted on the computerised numerical controlled machine (CNC) Simple Turn 5075SPM lathe. For experiments, carbide-coated inserts ISO designation KC5010 for PVD; CNMG120408-MP with an appropriate tool holder under MQL condition were used. When turning Inconel 800H alloy, cutting parameters such as cutting speed, feed rate, nozzle distance, and nozzle angle were varied, as presented in Table 1. Throughout the experiment, the depth of cut was kept /maintained at 0.5 mm. Taguchi's L_{27} orthogonal array was chosen as the proper experimental design for factors and levels (presented in Table 1). The output responses of the experiments are surface roughness (R_a), cutting force (F_z), and residual stress (Res). Table 2 presents an overview of the parameters applied in the trials and experimental outputs. The machining experiment was carried out under MQL conditions for a cutting length of 10 mm. The flow rate of the MQL was fixed as 50 ml/hr at the pressure of 4 bar during all experiments. Furthermore, the schematic view of the complete process flow, including the pre and post-experiments used in the present work, is shown in Figure 1. A small amount of cutting fluid was mixed with compressed air into the mixing chamber to form an atomised fluid using a positive displacement pump in the MQL system. The fluid chamber delivered compressed air and oil. The airflow valve regulates air quantity, and the frequency generator controls the pumping cycle. Micro-nozzles were employed to supply the atomised fluid and were targeted on the cutting tool's edge. In the present MQL delivery system, the nozzle angle and distance can be varied. For nanofluids preparation, a two-stage mixing process was employed. Following this, hBN particles with an average particle size of 50 nm were added to olive oil in a proportion (0.2% weight concentration), as previously estimated through knowledge of the literature (Vasu and Pradeep Kumar Reddy, 2011). And it was subjected to a series of mixing processes. Olive oil and nanoparticles were first combined in a sonicator for 60 minutes at a pulse rate of 3 seconds before the subsequent phases in the mixing procedure. A magnetic stirrer was used to stir nanofluids for 60 minutes. Herein, nano additives are distributed homogeneously in olive oil. As a result, the fresh nanofluids obtained, the prepared nanofluid was stable, and no signs of sedimentation were detected throughout the machining process. Fluid properties such as dynamic viscosity, surface tension, wetting behaviour, and thermal conductivity significantly impact fluid performance. As a result, substantial knowledge about the nanofluid and its thermo physical properties was required. The viscosity of 0.20 wt.% hBN nanofluids was measured with a redwood viscometer. The kinematic viscosity at three temperatures of 40, 50, and 60°C was 2.04×10^{-6} m^2/sec, 1.45×10^{-6} m^2/sec, and 1.20×10^{-6} m^2/sec. A piezoelectric dynamometer (Kistler type 9257B) was applied to measure the cutting force during the experiments. Surface roughness measuring instrument (brand: MAHR; Model: MarSurf PR200) used to measure surface roughness. The residual stress on the sample was measured using an instrument (Pulstec X360) residual stress analyser based on the non-destructive X-ray diffraction method.

Table 1 Cutting parameter of Inconel 800H

Parameters	*Values*
Cutting velocity (V_c, m/min)	70–210 m/min
Feed (f. mm/rev)	0.1–0.2 mm/rev
Spraying angle (θ °)	15–45 °
Spraying distance (L, mm)	4–12 mm

2.1 Multi-objective optimisation

Optimisation techniques were primarily used to maximise or minimise the variables in its design range. Optimisation methods identify the optimal parameter for numerous complex engineering problems. In this present research work, HHO's main objective is to predict the optimal input values based on population sise and the number of search agents. TOPSIS, one multi-criteria decision-making method (MCDM), was used to rank the best possible solution obtained in non-dominated solutions from HHO (Abbasi et al., 2021). Therefore, multi-objective optimisation coupled with MCDM was incorporated in this research to determine optimum machining parameters.

2.2 Statistical evaluation of the experimental data

An analysis of variance (ANOVA) tool was used to investigate the experimental parameters' influence on output responses. The ANOVA provides several crucial aspects of statistics, including the (SS) sum of squares, (MS) the mean square, (DF) degree of freedom, the P-value, and the F value. On the other hand, the RSM presents an overview of a numerical model that relates the machining parameters (Vc, f, θ, and d) and the machining responses (R_a, F_z, Res). The RSM model can be quadratic or linear. The performance assessment test of ANOVA, which determines whether the RSM models are adequate, justifies the established models (Sen et al., 2019). In this particular investigation, the (RMSE) root mean square error, (MAPE) mean absolute percentage error and the (R^2) coefficient of determination are all utilised in the process of determining the amount of difference that occurs between predicted values (P_i) and experimental values (E_i).

Table 2 Experimental inputs and outputs

Sl. no.	*Cutting velocity (V_c, m/min)*	*Feed rate (f, mm/rev)*	*Nozzle angle (θ°)*	*Nozzle distance (L, mm)*	*Surface roughness (R_a μm)*	*Cutting force (F_z, N)*	*Residual stress (Res, MPa)*	*Nose wear (V_n, μm)*	*Flank wear (V_b, μm)*
1	70	0.1	15	4	0.67	133.00	378.00	20.08	37.23
2	70	0.1	30	8	0.39	127.60	521.00	20.09	38.33
3	70	0.1	45	12	0.27	123.50	423.00	20.08	25.55
4	70	0.15	15	8	0.85	152.30	549.00	44.20	40.56
5	70	0.15	30	12	0.86	169.40	647.00	48.22	50.68
6	70	0.15	45	4	0.88	145.80	480.00	52.24	55.32
7	70	0.2	15	12	0.87	182.10	445.00	68.43	68.53
8	70	0.2	30	4	1.55	214.70	519.00	68.31	66.49
9	70	0.2	45	8	0.97	191.60	423.00	56.22	69.81
10	140	0.2	15	4	1.57	77.98	600.00	56.22	86.001
11	140	0.2	30	8	1.56	177.70	686.00	84.38	93.68
12	140	0.2	45	12	1.42	157.40	707.00	76.40	95.94
13	140	0.1	15	8	0.37	51.67	337.00	28.13	42.31
14	140	0.1	30	12	0.39	111.30	646.00	32.15	42.58
15	140	0.1	45	4	0.39	70.45	387.00	36.14	42.50
16	140	0.15	15	12	1.01	138.40	671.00	52.24	63.50
17	140	0.15	30	4	0.79	125.96	614.00	50.58	72.39
18	140	0.15	45	8	0.77	126.50	550.00	32.15	59.62
19	210	0.15	15	4	0.78	58.25	548.00	68.31	81.14
20	210	0.15	30	8	0.93	138.20	614.00	66.31	72.10
21	210	0.15	45	12	0.52	114.60	486.00	68.31	89.43
22	210	0.2	15	8	1.55	98.90	761.00	80.36	94.01
23	210	0.2	30	12	1.39	168.60	608.00	88.40	103.26
24	210	0.2	45	4	1.38	154.60	648.00	88.40	81.07
25	210	0.1	15	12	0.68	101.90	305.00	52.21	74.33
26	210	0.1	30	4	0.64	89.93	452.00	56.22	63.75
27	210	0.1	45	8	0.47	97.51	373.00	60.27	63.75

Figure 1 Preparation of nanofluid, experimental setup, measurement, and optimisation (see online version for colours)

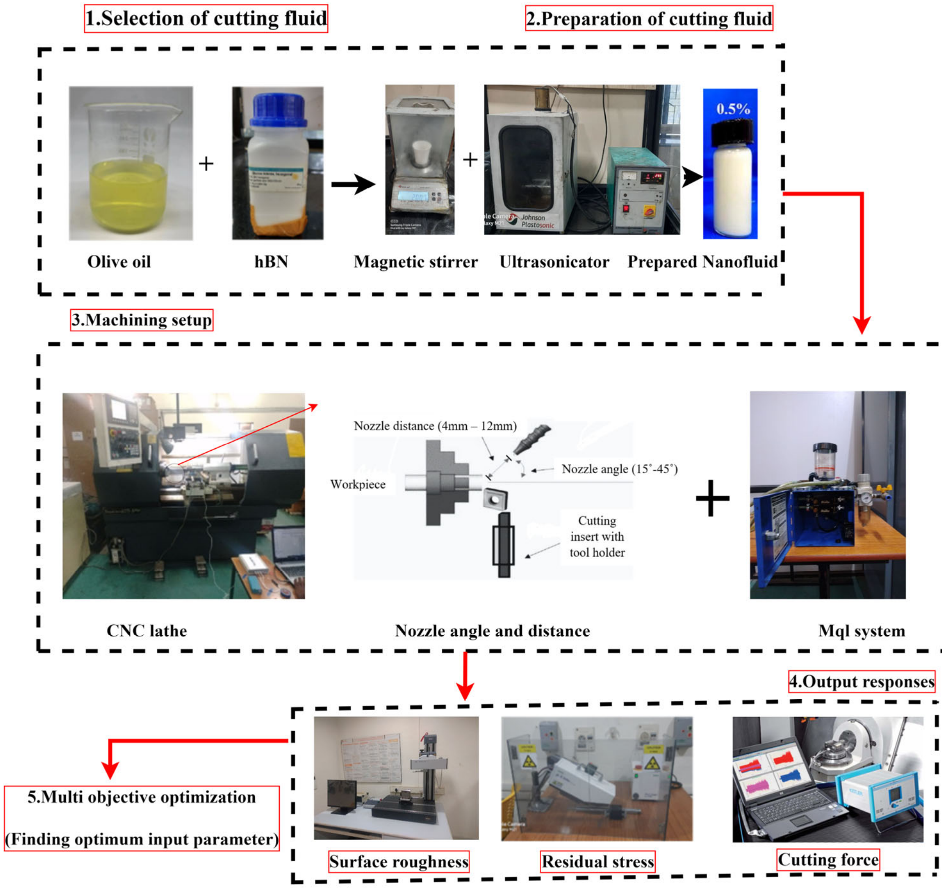

2.3 Harris hawks optimisation

Heidari et al. (2019) developed the optimisation algorithm known as HHO. It is an optimisation method inspired by Harris hawk birds' nature and behaviour modelling. In terms of performance, quality of results, and acceptable convergence in dealing with various applications in real-world situations, the HHO has gotten a lot of attention from researchers. The HHO algorithm includes the exploration and exploitation phases, which mimic the natural hunting habits of Harris hawks. In this algorithm, a group of hawks targets a hunt to surprise it (exploration phase). When escaping and fleeing the hunt, the Hawks can undertake a series of fast dives close to the target to startle it and exhaust it (exploitation phase). The running process can significantly reduce the energy of the prey. The HHO algorithm can switch from the exploring phase to the exploit phase depending on the escaping energy of that prey and then move between different opportunistic modes.

$$X(t+1)=\begin{cases} X_r(t)-r_1\left|X_r(t)-2r_2X(t)\right| & q\geq 0.5 \\ X_b(t)-X_m(t)-r_3\left(LB+r_4(UB-LB)\right) & \text{otherwise} \end{cases} \tag{1}$$

$$E=2Eo\left(1-\frac{itera}{itera_{\max}}\right) \tag{2}$$

The prey's energy model has given above, where E stands for the energy of the prey's running and fleeing at each iteration. The initial energy of prey is E_0, and the value of E_0 varies between (–1 to 1). The user gives iteration maximum value. E_0 fluctuates randomly within the range (–1 to 1) at each cycle. The prey is exhausted when the E_0 value decreases from 0 to –1; when the E_0 value rises from 0 to 1, the prey strengthens. During iterations, the prey's stamina for escaping from Harris hawks usually fades away. When $|E| \geq 1$, the hawks look in different sites to make the prey's position, and the HHO is in charge of the exploration phase. When $|E| < 1$, on either hand, the exploitation phase is performed on the HHO. The HHO (Heidari et al., 2019) presents four strategies for the mathematical model to attack the prey based on its running ways and the chasing trends of the Harris hawks. These strategies are:

1 hard besiege with progressive rapid dives

2 soft besiege

3 hard besiege

4 soft besiege with progressive rapid dives.

Table 3 Conditions for different strategies used in exploitation phases

Different strategies	*Conditions*	*Mathematically formula*	*Equations*
Soft besiege	C1: $\lvert r\rvert \geq 0.5$ and $\lvert E\rvert \geq 0.5$	$X(t+1)=\Delta X(t)-E\left\lvert J * X_b(t)-X(t)\right\rvert$	(3)
		$\Delta X(t)=X_b(t)-X(t) \quad J=2(1-r_5)$	(4)
Hard besiege	C2: $\lvert r\rvert \geq 0.5$ and $\lvert E\rvert < 0.5$	$X(t+1)=X_b(t)-E\left\lvert\Delta X(t)\right\rvert$	(5)
Soft besiege with progressive rapid dives	C3: $\lvert r\rvert<0.5$ and $\lvert E\rvert \geq 0.5$	$X(t+1)=\begin{cases} Y \text{ if } Fit(Y)<Fit(X(t)) \\ Z \text{ if } Fit(Z)<Fit(X(t)) \end{cases}$ $Y=X_b(t)-E\left\lvert J * X_b(t)-X(t)\right\rvert$ $Z=Y+S * levy(D)$	(6)
Hard besiege with progressive rapid dives	C4: $\lvert r\rvert <0.5$ and $\lvert E\rvert < 0.5$	$X(t+1)=\begin{cases} Y \text{ if } Fit(Y')<Fit(X(t)) \\ Z \text{ if } Fit(Z')<Fit(X(t)) \end{cases}$ $Y'=X_b(t)-E\left\lvert J * X_b(t)-X_m(t)\right\rvert$ $Z'=Y'+S * levy(D)$	(7)

Notes: J is the random jump strength of the rabbit which used to escape from the hawks.
r_5 is a random value created from the interval [0, 1].
levy (D) is the levy flight function with dimension D.
D is the dimension of the optimisation problem to be solved.
S is the random vector by size ($S \in R^{1\times D}$).

Figure 2 Methodology for proposed work (see online version for colours)

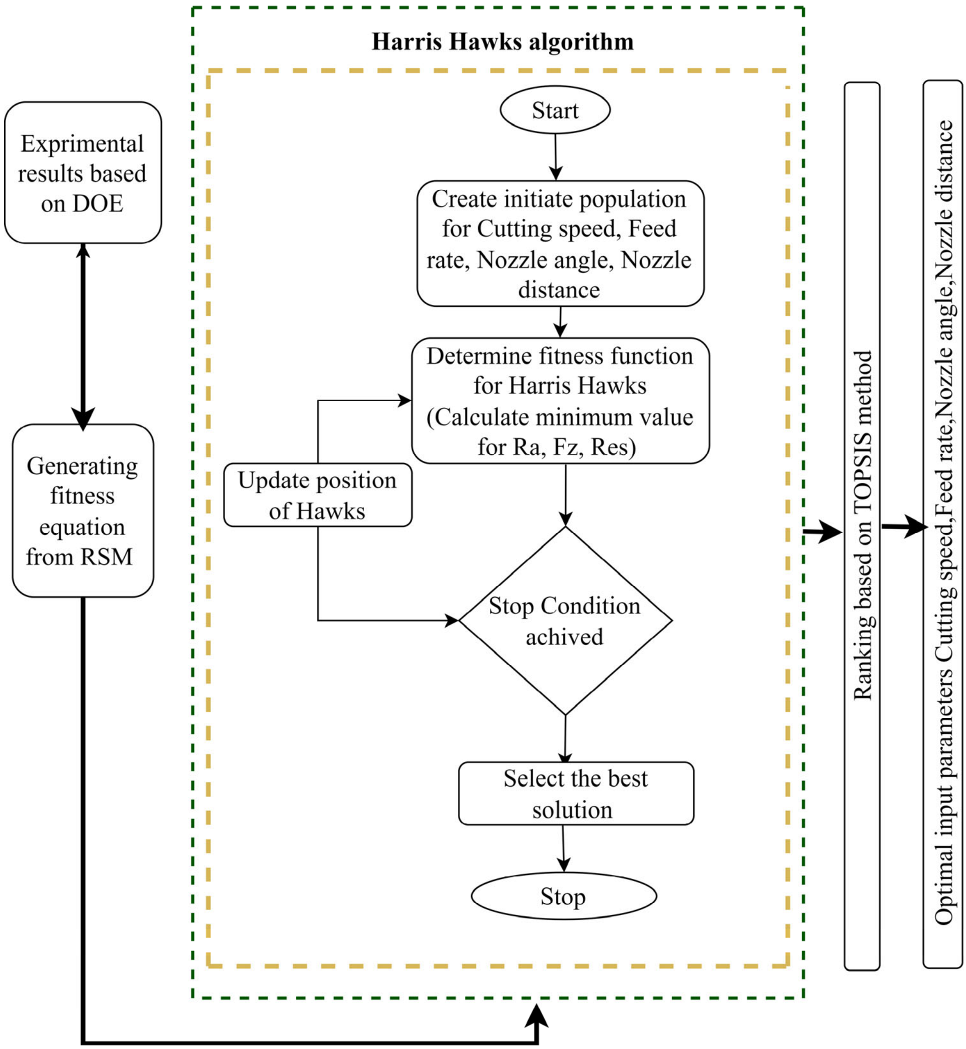

2.4 TOPSIS method

TOPSIS is one of the MCDMs, which is exploited to find the Relative closeness index or criterion (Hussain et al., 2018). In this work, TOPSIS is coupled with HHO to rank the non-dominated solutions into a single solution (Deb et al., 2016). TOPSIS applied to choose the best replacements by reducing the distance to the ideal positive result and increasing the distance to the negative result, where all alternates are ranked based on their closeness index.

Step 1 Formation of decision matrix.

Identify the objective and the assessment features or responses that are pertinent to it. For example, the decision matrix is depicted in equation (8).

$$D\left[x_{ij}\right]_{nxm} = \begin{bmatrix} x_{11} & x_{12} & . & x_{ij} & x_{1n} \\ x_{21} & x_{22} & . & x_{2j} & x_{2n} \\ . & . & . & . & . \\ x_{i1} & x_{i2} & . & x_{ij} & x_{in} \\ . & . & . & . & . \\ x_{n1} & x_{n2} & . & x_{nj} & x_{nm} \end{bmatrix} \tag{8}$$

Step 2 Calculating normalised values; using the vector normalisation method, compute the normalised decision matrix, B_{ij}, as shown in equation (9).

$$B_{ij} = \frac{x_{ij}}{\sqrt{\sum_{i=1}^{n} x_{ij}^2}} \qquad j = 1, 2, \ldots, m \tag{9}$$

Step 3 Calculating weights for responses. Weighted normalised matrix v_{ij} is obtained by multiplying each element by its affiliated weight (obtained by distinct weight methods). Normalised weighted matrix v_{ij} denoted by equation (11).

$$V_{ij} = W_j B_{ij} \quad \text{for} \quad i = 1, \ldots, n;\ j = 1, \ldots, m. \tag{10}$$

Step 4 Finding the ideal positive solution and ideal negative solution.

With equations (11) and (12), find the ideal (highest) and negative ideal (lowest) solutions (19). The ideal (highest) and negative ideal (lowest) solution for a given feature may be the largest or minimum value among all possible values.

$$A^- = \left(v_1^-, v_2^-, \ldots, \cdot v_m^-\right) = \left[\left(\min_i V_{ij} \middle| j\ \varepsilon\ I\right), \left(\max_i V_{ij} \middle| j\ \varepsilon\ I\right)\right] \tag{11}$$

$$A^+ = \left(v_1^+, v_2^+, \ldots, \cdot v_m^+\right) = \left[\left(\max_i V_{ij} \middle| j\ \varepsilon\ I\right), \left(\min_i V_{ij} \middle| j\ \varepsilon\ I\right)\right] \tag{12}$$

Step 5 Finding separation value from positive ideal and negative ideal solution.

Take the necessary separation measures (d_i). The distance between each alternative and the ideal one is known as the Euclidean distance.

$$d_i^+ = \left(\left[\sum_{j=1}^{m} \left(v_{ij} - v_j^+\right)^2\right]^{\frac{1}{2}}\right), \qquad i = 1, 2, \ldots, n \tag{13}$$

$$d_i^- = \left(\left[\sum_{j=1}^{m} \left(v_{ij} - v_j^-\right)^2\right]^{\frac{1}{2}}\right), \qquad i = 1, 2, \ldots, n \tag{14}$$

Step 6 Calculate relative closeness value: To determine how near an alternative is to the ideal solution by using that relative closeness (RC_i) formula shown below.

$$R_c = \frac{d_i^{*-}}{d_i^{*-} + d_i^{*+}} \tag{15}$$

3 Results and discussion

3.1 Statistical analysis of machining responses

As previously indicated, the ANOVA approach was used to determine the influence of each machining input response on machining. The F value was used to compute the percentage contribution of each component to machining outputs, and the P value less than 0.05 demonstrated the statistical importance of each element (Sen et al., 2019). The calculated ANOVA for all machining responses was established in Table A Appendix (added in Annexure A). ANOVA was accomplished to predict the influence of machining factors on surface roughness, cutting force, and residual stress. The contribution of a feed rate of 81.74%, nozzle angle of 2.74%, nozzle distance of 1.07%, and cutting speed of 0.57% for surface roughness. All input parameters are statistically substantial when the P value is considered. Then the F value shows that the feed rate was the most important component, followed by nozzle angle, nozzle distance, and cutting speed. The F-value indicates the feed rate affects the resultant force of cutting with 33.80%, followed by a cutting speed of 28.43%, nozzle angle of 13.87%, and nozzle distance of 4.86%. The ANOVA for residual stress is also implicit. The feed rate is the most contributing factor at 40.77%, followed by nozzle angle at 11.41%, cutting speed at 9.35%, and nozzle distance at 1.40%. The F-value in residual stress revealed dominance of feed rate.

3.2 Meta-modelling and performance evaluation

RSM is a popular statistical modelling and optimisation tool that finds a region around the optimal solution. As a result, RSM has been employed to develop the mathematical model correlation between cutting parameters and each process response, i.e., R_a, F_z, and Res. Despite the complexity of machining, the first-order linear equation cannot sufficiently validate the experimental study. As a result, in this work, RSM was developed using 2nd order equations with mutual connections for machining responses. [as shown in equations (16)–(18)]. Following that, RMSE, R^2, and MAPE are used to estimate the difference between RSM-predicted values and experimental values. Table 4 exposed that the RSM model prediction of cutting performances with experimental data yields RMSE ranges from 0.7652 to 0.8842%, R^2 ranges from 0.90124 to 0.92315, and MAPE ranges from 2.321 to 1.956%, demonstrating the effectiveness of the meta-model.

$$\begin{aligned}\mathrm{R_a} = {} & 0.42+0.00049\times c_v-3.7\times f+0.0202\times\theta-0.043\times L-0.000010\times c_v^2\\ & +38.9\times f^2-0.000390\times\theta^2+0.00118\times L^2+0.0118c_v\times f-0.000022c_v\\ & \times\theta+0.000253c_v\times L+0.0175f\times\theta-0.163f\times L-0.000144\times\theta\times L\end{aligned} \tag{16}$$

$$\begin{aligned}\mathrm{F_z} = {} & 97.7-1.844\times c_v+108f+5.49\times\theta+8.06\times L+0.00443c_v^2-0.1160\theta^2\\ & +0.00905c_v\times\theta+15.56f\times\theta-0.1778\theta\times L\end{aligned} \tag{17}$$

$$\begin{aligned}\mathrm{Res} = {} & -371+1.25\times c_v+6{,}337\times\theta+22.43\times\theta-0.01379c_v^2\\ & -24{,}422\times f^2-0.381\times\theta^2+19.57c_v\times\theta\end{aligned} \tag{18}$$

Table 4 Performance assessment of the RSM model on the statistical platform

Parameter	*RMSE (%)*	R^2	*MAPE (%)*
R_a (μm)	0.8012	0.91235	2.135
F_z (N)	0.7652	0.92315	2.321
Res(MPa)	0.8842	0.90124	1.956

3.3 *Influence of cutting conditions on machinability*

Figure 3(a) shows the one-dimensional main effect plot on cutting force (F_Z). As cutting speed increases, the overall value of cutting forces decreases. From Figure 3, it was detected that the lowest resultant cutting force was found at a cutting speed of 210 m/min. The increase in cutting force was observed with an increase in feed rate. The higher the cutting speed, the hotter the border amid the workpiece material and cutting tool. As a result, the shear strength of the cutting zone decreases, reducing the cutting force. While increasing the cutting speed decreases the tool chip contact area, resulting in low frictional force at the rake surface, thus reducing cutting force. The reduction in the growth of cutting force along with an increment of cutting speed is because of the energy balance between the thermal softening and strain-hardening rate. The strain-rate phenomenon of material can also explain this situation. The material surface becomes brittle facture behaviour as the strain-rate parameter increases, and after a certain speed, the material sensitivity to the speed grows uncertain. Thus, a decrease in cutting force is observed at a higher cutting speed. This consequently reduces the contact surface with the cutting tool and considerable friction. The observation is parallel with preceding surveys (Movahedi et al., 2020; Damir et al., 2017). Increasing the feed rate will increase the chip load per tooth, where an increased tendency of the resultant force is observed. During the turning process, the increase in feed rate results in a reduction in the oil mist penetration rate at the turning zone, resulting in an increase of friction at the too-chip interface part. Thus, the cutting force increased with the increment of feed rate under the MQL environment. Figure 3(a) shows the force increase with the nozzle angle and distance increment. The decrement cutting force of 45° is due to the bulk cooling that may be happened of MQL spray mist delivered at the turning zone. This bulk cooling is due to the diminished effect of splashing lubricating oil into the contact zone. Further, some portion of the lubricant droplet is deposited on the tool-work part interface at a higher value of the spraying angle of the nozzle. Therefore, effective lubrication occurs, and cutting force is minimum. The lubrication efficiency decreased with an increase in nozzle angle of 30°. At the 30° nozzle angle, a smaller amount of oil droplets penetrate the cutting surface. This eventually decreases the lubricant droplet's wetting ability and thus increases the cutting force. However, with the given air pressure and flow rate input, the nozzle distance and angle to the turning edge should be kept minimum to achieve lower cutting force. At these MQL conditions, nanofluids' deposition rate and penetration ability into the tool-work interface increased, resulting in decreased friction at the contact layer. The formation of the thin and strong lubricating layer at the tool-work edge brings down the cutting temperature due to friction heat. The combination of boron and nitrogen atoms arranged in the nanofluid has strong adhesive forces and provides an excellent lubricant film under high pressure. Hence lead to a lower machining force through the smaller value of impingement nozzle angle and distance under the MQL environment.

Figure 3(b) shows that increasing cutting speed decreases R_a. The lowest surface finish value was achieved at 70 m/min cutting speed. In effect, a higher cutting speed aids in softening the material by increasing the heat in the cutting zone. As a result, cutting at a lower temperature is possible at faster cutting speeds. However, the increment in R_a with an increase in cutting speed is minimal compared to the increase in feed rate. The irregular built-up edge (BUE) formed on the rake face at a higher cutting speed. The formed BUE [Figure 6(c)] pushes the tool from its original path, increasing the roughness value. An insignificant increase in surface roughness with an increment in cutting speed may be related to less mechanical load on the tooltip. In addition, the high thermal conductivity of hBN particles reduces the cutting temperatures at the cutting zone by giving effective cooling and lubrication actions. The formed thin film lubricant improves wettability and lowers friction at a higher cutting speed. As a result, it decreases the abrasion marks on the tool's surface. Hence, the increment in R_a value is very low at a higher cutting speed. In the same way, the increase in the feed rate increase of R_a vale. The lubricant effect of nanofluid at the cutting zone is ineffective with an increase in feed rate, which increases friction at the tool chip and works piece-tool junction regions. This could increase the R_a value by increasing the feed rate during the machining process. The tooltip region is subjected to a high cutting force when the feed rate value increases, producing a rougher surface finish. Finally, the mechanical load was increased, and the increased rubbing action negatively impacted the R_a at the tooltip and the lubricating oil being broken at a faster feed rate. The decrease of R_a with the given increment value of nozzle angle and distance is noticed when both nozzle orientation and spraying distance parameters are kept high. The difference in R_a value is insignificant when the spraying angle is at 15° and 30°. The oil mist does not completely penetrate the tool chip and workpiece's junction zones at these two positions. With the given air pressure and flow rate input, the increase of spraying angle to 45° reduce the droplet size and increase the number of droplets and velocities. This helps the nan fluid droplet to penetrate the contact zones efficiently, resulting in decreased friction at the contact area. Thus, consequently, it enhances the surface quality and cutting force when the spraying angle of the nozzle is at 45°. Likewise, the decrement in surface roughness with increment in spraying distance was noticed from the main effect plot of the spraying distance column. This reduction is due to droplet velocity and diameter concerning spraying distance. Moreover, the increment in spraying distance leads to higher droplet velocities; therefore, the penetration and deposition rate into the contact surface increases. Additionally, increasing the spraying distance decreases the droplet diameter and increases the lubrication efficiency. These results parallel the literature source (Movahedi et al., 2020; Mia, 2018; Kumar et al., 2019). Figure 4 shows the optical microscopic images of the machined surface with Trail 9, Trail 12, and Trail 27, along with the surface profile image captured with Mahr Surf. The machined surface morphology demonstrates that smoother and shallower groove (refer to 2D machined surface images) surfaces are observed at Trial 9. In other words, the surface irregularities using NFMQL conditions showed the peak and valley differences decreased when the nozzle angle was at 45°. For the same nozzle angle, the peak-to-valley height difference for Trail 12 decreased with the increased cutting speed. However, it was noticed that the difference between the peak-to-valleys height was very little climb as the cutting speed increased at a high spraying angle. The distinctive feed marks were reduced for Trail 27 with the NMQL system. The efficient operation of both C/L can explain this.

Figure 3 Effect of input values on (a) cutting force, (b) surface roughness, and (c) residual stress (see online version for colours)

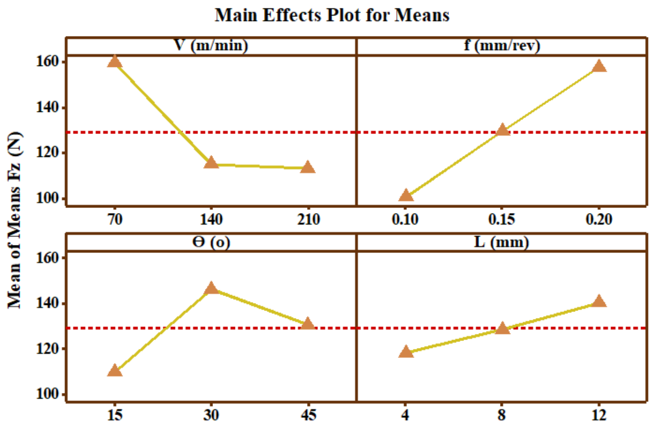

(a)

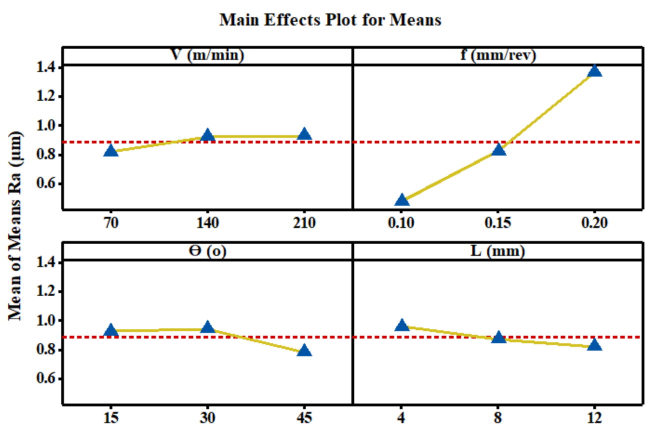

(b)

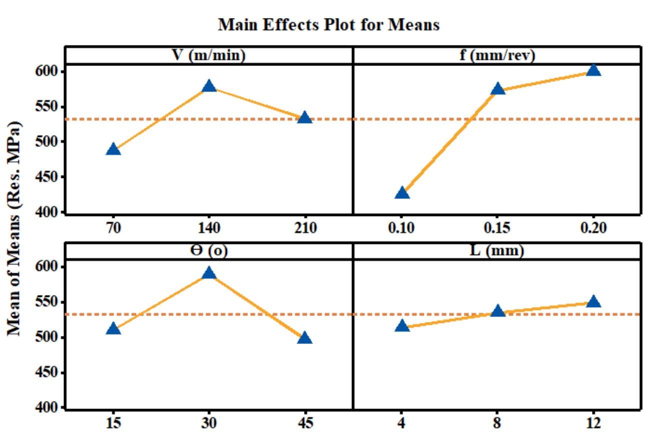

(c)

Figure 3(c) shows the one-dimensional mean effect on residual stress. The residual stress is tensile with the applied range of parameters. The variation in the magnitude of tensile residual stress is due to the cutting and lubrication parameters employed. The external surface is caused to deform plastically (plastic deformation) by compression during machining. Therm load is the main source of tensile residual stress on the surface layer. The graph's findings showed that tensile residual stress increased with an increment of cutting speed and feed rate. The lowest tensile residual is produced at 70 m/min. In addition, the penetration of nanofluid droplets in the tool-chip contact region at a low cutting speed significantly improves heat evacuation from the turning zone. As a result, it increases the work-hardened of the machined surface layer. The increase of tensile stress at 140 m/min is owed to a larger heat generation. With the shorter contact duration between the tool-work piece chip with the increment of turning speed, the generated heat is not removed through the produced chip. Instead, it results in the difference in cooling temperature between the surface and subsurface layer. This, in turn, will be led to tensile residual stress. The increase in cutting speed increases the cutting temperature and heat concentration into the turning zone owing to the lesser thermal conductivity of Inconel 800H. Hence, tensile residual stress is observed. Further, the PVD coatings are a thermal barrier, delaying the heat transfer tool. As a result, the generated heat near the primary zone is choked in the workpiece. The decrease of tensile residual stress at a higher cutting speed may be explained by the presence of more unsaturated fatty acids percentage (85%) in olive oil helps form a lubricant layer between the contact surfaces, as reported in a previous note (Talib et al., 2017). Further, the high heat conductive of hBN transmit a substantial quantity of the released heat from the turned layer. This, in turn, decreases the scale of tensile stress at the surface turned. Therefore, the cutting force and lower tensile residual stress are noticed at a higher cutting speed. The rise in feed rate increases the surface tension in the cutting direction. The increased pressure in the cutting direction cause it to grow in a more considerable compressive plastic deformation. The increase of tensile residual stress at a high feed rate is comparatively less than the moderate feed rate. From the mean effect graph, an increase in spraying angle from 15° to 30° increase the tensile stress and then decline with a further increase in nozzle angle. The lowest value of tensile residual stress is observed at 45°. The lubrication effect of the nanofluids increases at 45° due to the nanoparticle's effective deposition rate and penetration capability at the contact zones. The nanofluids form a consistent hydrodynamic film that separates the contact surface during machining and reduces the workpiece's thermal loads. Thus, frictional force reduces the surfaces in contact, leading to lessening tensile residual stress; hence, the lower cutting force and surface quality are observed when the spraying angle of the nozzle is at 45°. The larger droplet diameter with lower velocities reduces the thermal and mechanical load at a lower spraying angle. Thus the tensile stress at the surface turned is minimal compared to the 30° spraying angle. The increment in tensile residual stress with an increment in spraying distance is noticed from the main effect plot of the spraying distance column. Observing tensile residual stress at a given spraying distance is mostly contingent on the mechanical stress produced by cutting force during the turning process. The results parallel the literature source (Emami et al., 2013; Zaman and Dhar, 2020).

Figure 4 Surface roughness images with an optical microscope (see online version for colours)

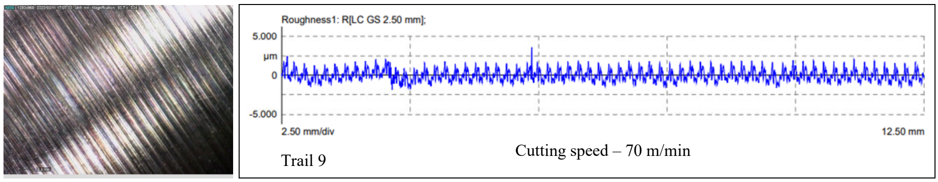

(a)

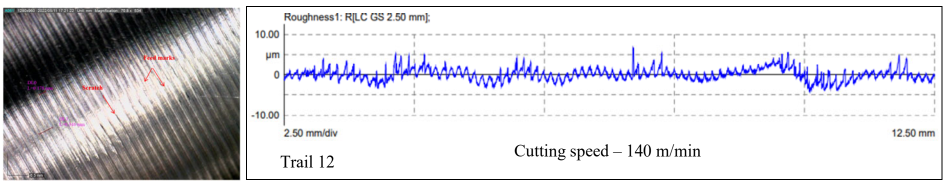

(b)

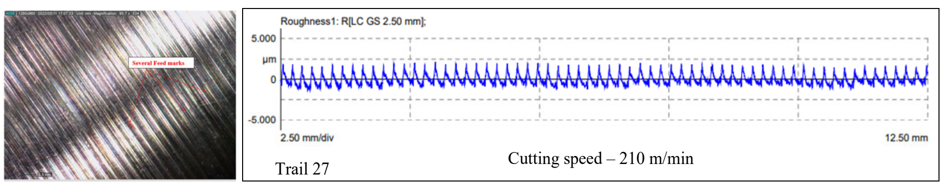

(c)

3.4 Correlation between the machining responses

The contour plots are more informative as it clearly shows the feasible region and the optimal point while measuring the effect of numerous independent factors that affect the response (Viswanathan et al., 2020). The contour effect plots [Figures 5(a)–(d)] were used to establish the influence of different machining conditions on surface roughness, cutting force, and residual stress values. The plots are drawn based on the highest contributing factor (ANOVA table) on the responses. Figure 5(a) contour effect plots show the surface roughness values were found to be maximum at high nozzle angle and feed rate values. Lower surface roughness values were observed at lower nozzle angles and feed rates. Figure 5(b) demonstrates that the lower magnitude of force was observed at a low feed rate and nozzle angle. This occurs because the nozzle's proximity to the cutting edge increases the overall mass of oil mist particles accumulated on the tool and chip contacts. A stronger lubricating effect will be produced during the material removal process when a greater amount of oil mist is penetrated the cutting zone. When the cutting tool and workpiece surfaces are properly lubricated, the frictional forces between them are reduced, which lowers the cutting forces needed to generate chips. The force value increased when the nozzle angle and feed rate value changed from low to moderate. In this position of nozzle angle, along with a low feed rate, more droplets of nanofluids were gusted away from the tool surface while the tool rotated systematically. In addition, the generated heat was not properly dissipated from the cutting zone because of the poor thermal conductivity of the alloy. Similarly, Figure 5(c) demonstrated that the higher feed rate and low cutting speed resulted in higher cutting force values. Figure 5(d) shows the contour plots of residual stress measurements for feed rate and nozzle angle for MQL conditions. The role of feed rate has more impact when equated with the cutting speed, nozzle distance, and nozzle angle. The observation results of these plots claim that the higher the feed rate, the higher the residual stress. Moreover, when increased feed rate depreciates the surface roughness value. This increment of tensile stress is due to a larger heat generation that prompts the higher residual stress. Nevertheless, at a feed rate of 0.1 mm/rev and a minimum nozzle angle of 15°, minimum residual stress of 450–500 MPa was obtained, and it inferred that the. A larger feed rate leads to higher residual stress. It may be due to increased spraying distance, which decreases the droplet diameter and thereby decreases the lubrication efficiency at the cutting zone. Thereby, the increase of residual stress on the machined surface. At a lower feed rate of 0.1 mm/rev and nozzle distance of 12 mm, the minimum value of residual stress is obtained. However, it may be due to increased spraying distance, which decreases the droplet diameter, increases lubrication efficiency, and encourages lesser residual stress.

Figure 5 Represents of contour plot for machining responses on (a) surface roughness, (b, c) cutting force (b,c), and (d) residual stress (see online version for colours)

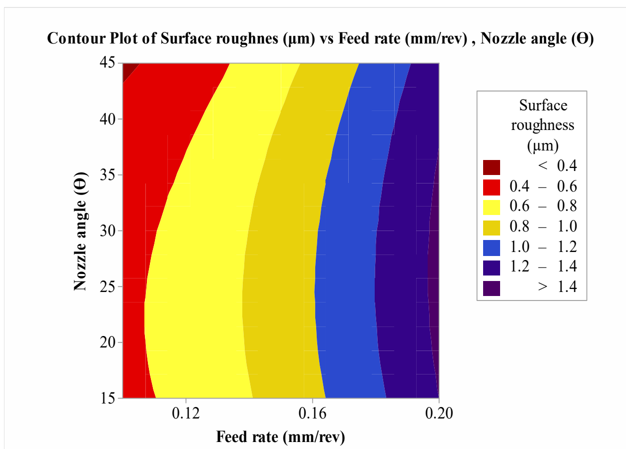

(a)

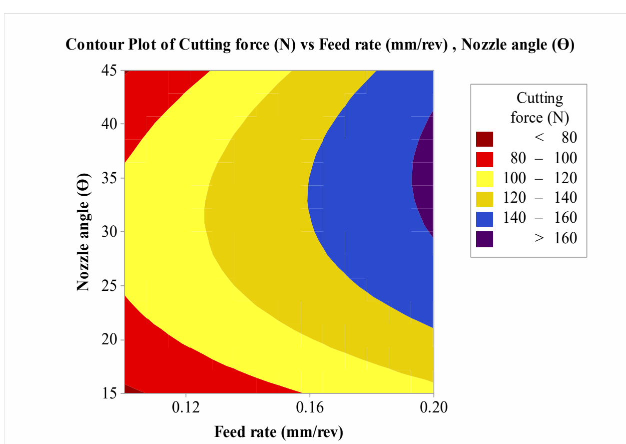

(b)

Figure 5 Represents of contour plot for machining responses on (a) surface roughness, (b, c) cutting force (b,c), and (d) residual stress (continued) (see online version for colours)

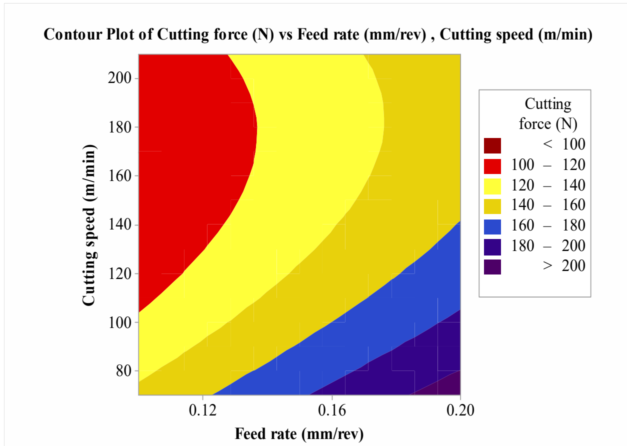

(c)

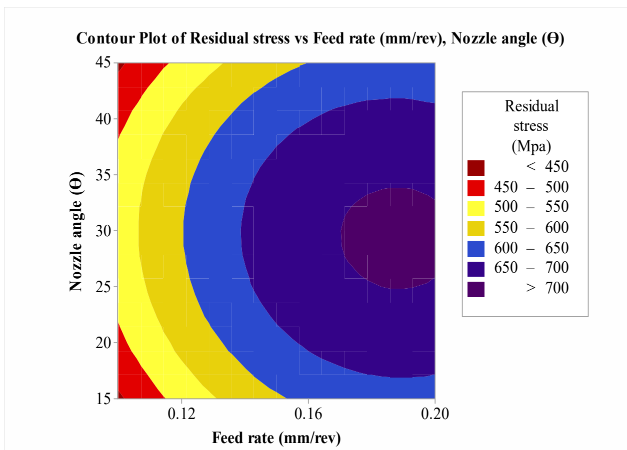

(d)

3.5 *Effect of tool wear*

In the current work, cutting tool wear is one of the selected objectives under MQL conditions. Cutting tool wear is the most basic indicator of a tool's lifespan and refers to material deterioration in the contact region between tool-work material (Ross et al., 2022b). For every experimental trial, nose and flank wear was measured with a Dinolite optical image analyser, and their values were presented in Table 2. Micro-optical images of nose and flank wear are shown in Figures 6(a)–6(d). The nose (29.84 μm) and flank wear (43.26 μm) were observed to lower at low cutting speed and feed. nMQL has two important characteristics in these MQL conditions. The first one was the less frictional impact, and the second reduced temperature (at a lower speed). With MQL, hBN was used to enhance efficient heat transfer. However, the fact that the hBN lowers the MQL fluid's temperature makes this nMQL approach work so well. Because of this, despite the tremendous heat in the cutting area, the droplets do not evaporate. For increased cutting speed and feed rate, flank wear and nose wear were increased by 88.40 µm and 103.26 µm, respectively. This is because the rising heat causes nMQL to lose its lubricating ability. As a result, the oil droplets vanish before it reaches the work-tool connection. The flank and nose wears were 51.48 µm and 63.08 µm, respectively, when the nozzle angle was lower, and the nozzle distance was moderate. This shows that the penetrating ability of nMQL oil mist significantly provided sufficient C/L action at the main turning zone, thereby reducing produced temperature. As a result, the tool flank and nose wear were decreased. Figure 6(b)–6(d) represents trails 11 and 22, where abrasion, adhesive/built-up-edge (BUE), and chipping were found as the basic wear mechanism for all tuning conditions. Abrasive wear lines occurred along the cutting edge due to the abrasive wear mechanism, forming parallel grooves that lead to flank wear. BUE formation on the cutting insert was due to temperature and a high friction coefficient. When the cutting speed and feed rate were increased, the lubricating property had little influence. Before the nanofluid gets to the cutting area, the nanofluid vaporises. Periodically, unstable BUE causes small amounts of tool material to be removed, which causes the cutting edge to chip. For the experimental inputs, it was observed that the lower amount of flank wears by 25.50 µm and nose wear by 20.08 µm were observed at 70 m/min, 0.1 mm/rev, 15°, and 8 mm. The MQL approach lowers friction and inhibits heat build-up by covering the tool-chip interface with a thin oil film, as was indicated in earlier investigations (Damir et al., 2017; Kannan and Kannan, 2018).

Figure 6 (a) Flank wear and nose wear for 27 trials (b) Flank wear at Trial 11 (c) Flank wear at Trial 22 (d) Nose wear at Trial 22 (see online version for colours)

(a)

Figure 6 (a) Flank wear and nose wear for 27 trials (b) Flank wear at Trial 11 (c) Flank wear at Trial 22 (d) Nose wear at Trial 22 (continued) (see online version for colours)

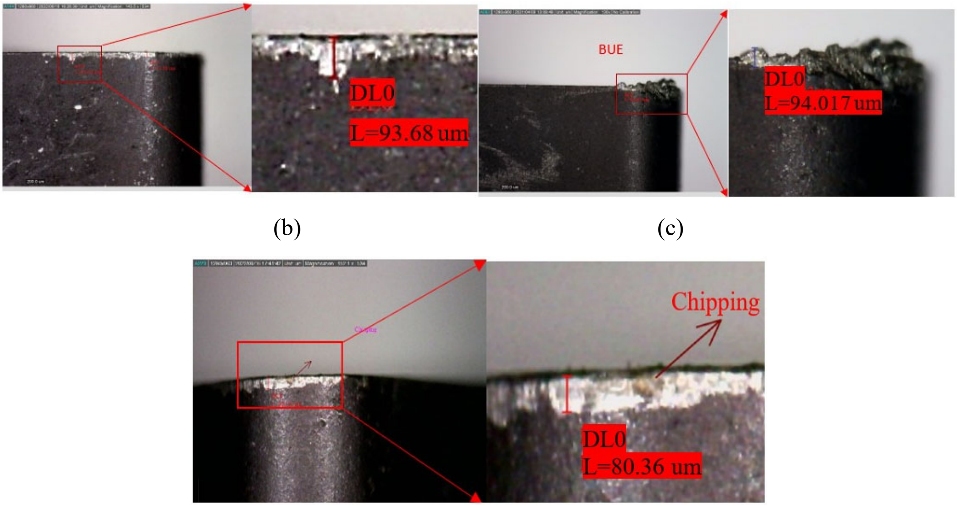

(b) (c)

(d)

3.6 *Optimisation and validation of results*

The results of the experimental work's machining trials completely satisfied the necessities of the computational optimisation study. A computational experiment with 100 populations and 100 generations was completed to evaluate the stability of the generated Pareto results. Additionally, total solutions in various parametric combinations underwent the validation test. Three similar investigations were conducted, and the mean value was noted. The validation test agrees with the relative error being less than 5%, demonstrating the HHO model's intelligence. This allows quantitatively determining the relationship between the machining parameters and their reactions. Table 5 shows the optimisation parameters of the HHO algorithm. The Pareto front had a hundred optimum options, but none could be called the best solution. However, the contradictory nature of the alternatives prevents researchers from choosing the best optimal solution. As a result, the TOPSIS technique was used to determine the optimal compromise solution. TOPSIS approach is heavily reliant on the relative importance of the objectives. As a result, the assignment of equal weightage to each target was fixed. Furthermore, the values of Rc_i were calculated using the values of D_i^+ and D_i^- to find the rank of the hundred optimal results detected. For the current challenge, a lower Rc_i number resulted in a higher rank. As a result, the 17th generation ranks top among the 100 generations. The best result attained by the TOPSIS method is shown in Figure 7. The best results correspond to cutting speed as 70 m/min, feed rate as 0.1 mm/rev, nozzle angle as 45$^{\theta}$, and nozzle distance as 12 mm, which gives minimum R_a (0.2377 μm), F_z (144 N), and Res (360 MPa). In addition, experimental trials were conducted at optimal conditions to validate the predicted responses. Table 6 shows the differences between the experimental and projected response values. The comparison reveals that the error percentage (RMSE) produced between the predicted and experimental responses were approximately 10.79%, proving the validity of the optimal parametric order. Compared to experimental values, the HHO predicted values showed an error percentage in R_a of 16.21%, F_z by 4.86%, and Res by 11.3%. To test the efficiency of the HHO algorithm, the same optimisation is done with some powerful leading algorithms. Comparative results are given in Table 7. Due to its strong exploration and search pattern, HHO could find solutions based on stability and steadiness between diversification and strengthening. Comparing it to other algorithms, it also converges close to the global optimum without getting trapped at the expense of the confined local optimal solutions. The HHO-TOPSIS showed an improvement in convergence rate by 9.57 %, 12.04 %, 11.73 %, and 32.65 % at the optimal determined values compared to other hybrid algorithms (NSGA-II, PSO, GA, and MFA).

Table 5 The optimisation parameters

Parameters	*Values*
Number of search agents	25
β	2
Number of iterations	200
Mutation rate	0.1
Inertia weight	0.5
Population size	100

Figure 7 Best solution obtained with TOPSIS-HHO (see online version for colours)

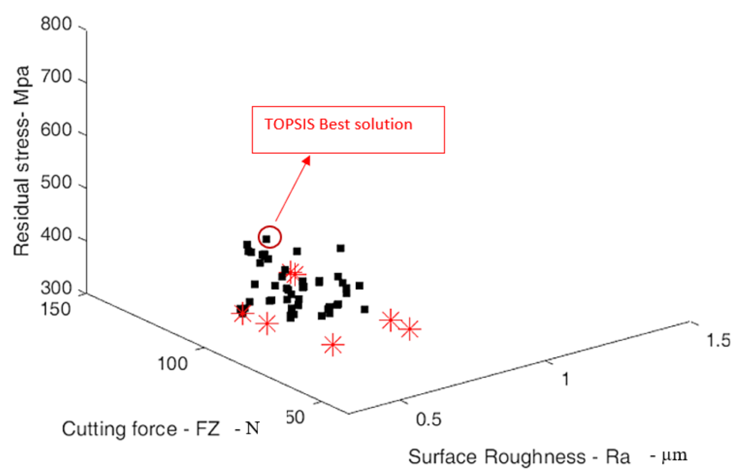

Table 6 Assessment of the predicted results and experimental results

Response parameters	*Optimised parameters*	*Experiment values*	*Values predicted*	*Errors (%)*
R_a (µm)	V_c =70 m/min, f = 0.1 mm/rev, angle = 45°, distance = 12 mm	0.2837	0.2377	16.21
F_z (N)		137	144	4.86
Res (MPa)		406	360	11.3
Error average = 10.79				

Table 7 Comparison of optimum design variables with other techniques

Algorithms	*HHO*	*NSGA-II*	*PSO*	*GA*	*MFA*
Best rank achieved	18	8	23	25	38
Rc_i values	0.1256	0.1389	0.1428	0.1423	0.1865
Errors (%)		9.57 %	12.04 %	11.73 %	32.65 %

4 Conclusions

An experiment trial was carried out on a CNC-lathe machine with the MQL technique on the machining performances of Inconel 800H alloy. Taguchi's L_{27} orthogonal array was used to frame the experimental design combinations to reduce the experimental effort. The best combination for obtaining the lowest value of the R_a-F_z and Res was determined by incorporating the combination of the HHO and TOPSIS hybrid algorithms. The effectiveness of hybrid HHO-TOPSIS was compared with other benched-marked algorithms. The subsequent conclusions drawn from the present study were:

- At the 90% confidence level, the constructed ANOVA models were shown to be statistically significant. Furthermore, the feed rate was the most important element influencing machining outputs, accounting for 81.74% of the reduction in surface roughness, 33.80% of the reduction in resulting cutting force, and 40.77% of the reduction in residual stress.
- The RSM technique successfully advanced a relationship between input parameters and machining responses and revealed RMSE ranges from 0.7652 to 0.8842%, R2 ranges from 0.90124 to 0.92315, and MAPE ranges from 2.321 to 1.956%.
- The main effect plot study reveals that the optimal input variables for minimising R_a are cutting speed 70 m/min, feed rate 0.1 mm/rev, nozzle angle 45°, and nozzle distance 12 mm. The F_z was reduced at a cutting speed of 210 m/min, feed rate of 0.10 mm/rev, nozzle angle of 15°, and nozzle distance of 12 mm. Similarly, the minimum residual stress was recorded with a cutting speed of 70 m/min, feed rate of 0.10 mm/rev, nozzle angle of 45°, and nozzle distance of 4 mm.
- The increment of MQL parameters of nozzle angle and distance increases the value of force and tensile residual stress and decrement in case roughness value when cutting speed and federate is kept at a higher and lower value.
- TOPSIS identified the most optimal outcomes from a Pareto front generated by HHO. The optimum solution corresponds to cutting speed at 70 m/min, feed rate of 0.1 mm/rev, nozzle angle at 45°, and nozzle distance of 12 mm, which gives minimum R_a (0.2377 μm), F_z (144 N), and Res (MPa).
- When the predicted results were compared to the experimental results, the error percentage was approximately 10.79%. The HHO predicted values showed an error percentage in R_a of 16.21%, F_z by 4.86%, and Res by 11.3% compared to experimental values. The HHO-TOPSIS showed an improvement in convergence rate by 9.57 %, 12.04 %, 11.73 %, and 32.65 % at the optimal determined values compared to other hybrid algorithms (NSGA-II, PSO, GA, and MFA).

- The proposed HHO-TOPIS is recommended for other machining processes to determine the most sustainable and eco-friendly solution.

Limitation, future scope, and implications

1. The present study will be extended for a detailed investigation of machinability indices and chip-tool interface indices (chip thickness, shear angle, coefficient friction) by considering the other oil-mist parameters, such as nozzle diameter, oil flow rate, and air pressure.
2. Machinability predictions for tool wear and cutting temperature can be implemented with the proposed hybrid optimisation algorithm.
3. Future research endeavors might be to evaluate the performance of hybrid optimisation coupled with ANN for better prediction accuracy instead of using RSM.
4. The performance of other machining approaches can be investigated by implementing the texture on the rake and flank face with different C/L conditions.
5. The effect of nozzle angle, distance, and machining parameters on surface integrity, such as microhardness and chip morphology, can be carried out.

Funding

The authors thank Vellore Institute of Technology for providing 'VIT SEED GRANT-SG20210179' for carrying out this research.

References

Abbasi, A., Firouzi, B. and Sendur, P. (2021) 'On the application of Harris hawks optimization (HHO) algorithm to the design of microchannel heat sinks', *Engineering with Computers*, Vol. 37, No. 2, pp.1409–1428.

Angappan, P., Thangiah, S. and Subbarayan, S. (2017) 'Taguchi-based grey relational analysis for modeling and optimizing machining parameters through dry turning of Incoloy 800H', *Journal of Mechanical Science and Technology*, Vol. 31, No. 9, pp.4159–4165.

Byrne, G. and Scholta, E. (1993) 'Environmentally clean machining processes – a strategic approach', *CIRP Annals*, Vol. 42, No. 1, pp.471–474.

Damir, A., Sadek, A., Attia, H. and Tendolkar, A. (2017) 'Characterization and optimization of machinability and environmental impact of machining of Ti-6Al-4V with minimum quantity lubrication', *International Journal of Robotics and Mechatronics*, Vol. 4, No. 1, pp.1–7.

Deb, M., Debbarma, B., Majumder, A. and Banerjee, R. (2016) 'Performance-emission optimization of a diesel-hydrogen dual fuel operation: A NSGA II coupled TOPSIS MADM approach', *Energy*, Vol. 117, No. 1, pp.281–290.

Elsheikh, A.H., Muthuramalingam, T., Shanmugan, S., Ibrahim, A.M.M., Ramesh, B., Khoshaim, A.B., Moustafa, E.B., Bedairi, B., Panchal, H. and Sathyamurthy, R. (2021) 'Fine-tuned artificial intelligence model using pigeon optimizer for prediction of residual stresses during turning of Inconel 718', *Journal of Materials Research and Technology*, Vol. 15, No. 1, pp.3622–3634.

Emami, M., Sadeghi, M.H. and Sarhan, A.A. (2013) 'Investigating the effects of liquid atomization and delivery parameters of minimum quantity lubrication on the grinding process of Al_2O_3 engineering ceramics', *Journal of Manufacturing Processes*, Vol. 15, No. 3, pp.374–388.

Gupta, M.K. and Sood, P.K. (2017) 'Machining comparison of aerospace materials considering minimum quantity cutting fluid: a clean and green approach', *Proceedings of the Institution of Mechanical Engineers, Part C: Journal of Mechanical Engineering Science*, Vol. 231, No. 8, pp.1445–1464.

Han, F., Li, L., Cai, W., Li, C., Deng, X. and Sutherland, J.W. (2020) 'Parameters optimization considering the trade-off between cutting power and MRR based on linear decreasing particle swarm algorithm in milling', *Journal of Cleaner Production*, Vol. 262, No. 1, p.121388.

Hegab, H., Salem, A., Rahnamayan, S. and Kishawy, H.A. (2021) 'Analysis, modeling, and multi-objective optimization of machining Inconel 718 with nano-additives based minimum quantity coolant', *Applied Soft Computing*, Vol. 108, No. 1, p.107416.

Hegab, H., Umer, U., Soliman, M. and Kishawy, H.A. (2018) 'Effects of nano-cutting fluids on tool performance and chip morphology during machining Inconel 718', *The International Journal of Advanced Manufacturing Technology*, Vol. 96, No. 9, pp.3449–3458.

Heidari, A.A., Mirjalili, S., Faris, H., Aljarah, I., Mafarja, M. and Chen, H. (2019) 'Harris hawks optimization: algorithm and applications', *Future Generation Computer Systems*, Vol. 97, No. 1, pp.849–872.

Huang, S., Lv, T., Wang, M. and Xu, X. (2018) 'Effects of machining and oil mist parameters on electrostatic minimum quantity lubrication – EMQL turning process', *International Journal of Precision Engineering and Manufacturing-Green Technology*, Vol. 5, No. 2, pp.317–326.

Hussain, S.A.I., Mandal, U.K. and Mondal, SP (2018) 'Decision maker priority index and degree of vagueness coupled decision making method: a synergistic approach', *International Journal of Fuzzy Systems*, Vol. 20, No. 5, pp.1551–1566.

Jeevan, T.P. and Jayaram, S.R. (2018) 'Performance evaluation of jatropha and pongamia oil based environmentally friendly cutting fluids for turning AA 6061', *Advances in Tribology*, Vol. 2018, No. 1, Article ID 2425619.

Kannan, V. and Kannan, V.V. (2018) *Empirical and Artificial Neural Network Modeling of Laser Assisted Hybrid Machining Parameters of Inconel 718 Alloy (No. 2018-28-0023)*, SAE Technical Paper.

Korkmaz, M.E., Gupta, M.K., Boy, M., Yaşar, N., Krolczyk, G.M. and Günay, M. (2021) 'Influence of duplex jets MQL and nano-MQL cooling system on machining performance of Nimonic 80A', *Journal of Manufacturing Processes*, Vol. 69, No. 1, pp.112–124.

Kumar, S., Singh, D. and Kalsi, N.S. (2019) 'Investigating the effect of approach angle and nose radius on surface quality of Inconel 718', *Journal of the Institution of Engineers (India): Series C*, Vol. 100, No. 1, pp.121–128.

Liu, Z.Q., Cai, X.J., Chen, M. and An, Q.L. (2011) 'Investigation of cutting force and temperature of end-milling Ti-6Al-4V with different minimum quantity lubrication (MQL) parameters'. *Proceedings of the Institution of Mechanical Engineers, Part B: Journal of Engineering Manufacture*, Vol. 225, No. 8, pp.1273–1279.

Majak, D., Olugu, E.U. and Lawal, S.A. (2020) 'Analysis of the effect of sustainable lubricants in the turning of AISI 304 stainless steel', *Procedia Manufacturing*, Vol. 43, No. 1, pp.495–502.

Mia, M. (2018) 'Mathematical modeling and optimization of MQL assisted end milling characteristics based on RSM and Taguchi method', *Measurement*, Vol. 121, No. 1, pp.249–260.

Movahedi, B., Mokhtari Homami, R. and Akhavan, S. (2020) 'A new approach of wear mechanism map in turning Inconel 718 with PVD-coated inserts using advanced techniques', *Iranian Journal of Science and Technology, Transactions of Mechanical Engineering*, Vol. 44, No. 4, pp.1091–1102.

Palanisamy, A. and Selvaraj, T. (2018) 'Optimisation of turning parameters on heat treated INCOLOY 800H using cryogenically treated CVD tool with grey-based entropy method', *International Journal of Machining and Machinability of Materials*, Vol. 20, No. 5, pp.401–424.

Palanisamy, A., Jeyaprakash, N., Sivabharathi, V. and Sivasankaran, S. (2021) 'Influence of heat treatment on the mechanical and tribological properties of Incoloy 800H superalloy', *Archives of Civil and Mechanical Engineering*, Vol. 21, No. 1, pp.1–15.

Rapeti, P., Pasam, V.K., Gurram, K.M.R. and Revuru, R.S. (2018) 'Performance evaluation of vegetable oil based nano cutting fluids in machining using grey relational analysis – a step towards sustainable manufacturing', *Journal of Cleaner Production*, Vol. 172, No. 1, pp.2862–2875.

Robinson Gnanadurai, R. and Mesfin, S. (2022) 'Investigations on the effect of silver nanoparticles on performance of coconut oil based cutting fluid in minimal fluid application', *Advances in Mechanical Engineering*, Vol. 14, No. 1, p.16878140211070445.

Ross, N.S., Ganesh, M., Srinivasan, D., Gupta, M.K., Korkmaz, M.E. and Krolczyk, J.B. (2022a) 'Role of sustainable cooling/lubrication conditions in improving the tribological and machining characteristics of Monel-400 alloy', *Tribology International*, Vol. 176, No. 1, p.107880.

Ross, N.S., Srinivasan, N., Amutha, P., Gupta, M.K. and Korkmaz, M.E. (2022b) 'Thermo-physical, tribological and machining characteristics of Hastelloy C276 under sustainable cooling/lubrication conditions', *Journal of Manufacturing Processes*, Vol. 80, No. 1, pp.397–413.

Rubaiee, S., Danish, M., Gupta, M.K., Ahmed, A., Yahya, S.M., Yildirim, M.B., Sarikaya, M. and Korkmaz, M.E. (2022) 'Key initiatives to improve the machining characteristics of Inconel-718 alloy: experimental analysis and optimization', *Journal of Materials Research and Technology*, Vol. 21, No. 1, pp.2704–2720.

Saleem, M.Q. and Mehmood, A. (2022) 'Eco-friendly precision turning of superalloy Inconel 718 using MQL based vegetable oils: tool wear and surface integrity evaluation', *Journal of Manufacturing Processes*, Vol. 73, No. 1, pp.112–127.

Salem, A., Hegab, H. and Kishawy, H.A. (2021) 'Holistic performance analysis during sustainable machining of Inconel 718 with minimum quantity lubrication-based nanofluids', *The International Journal of Advanced Manufacturing Technology*, Vol. 115, No. 7, pp.2219–2232.

Sen, B., Hussain, S.A.I., Mia, M., Mandal, U.K. and Mondal, SP (2019) 'Selection of an ideal MQL-assisted milling condition: an NSGA-II-coupled TOPSIS approach for improving machinability of Inconel 690', *The International Journal of Advanced Manufacturing Technology*, Vol. 103, No. 5, pp.1811–1829.

Singh, G., Aggarwal, V., Singh, S. and Singh, B. (2022) 'Sustainable machining of Hastelloy C-276 enabling minimum quantity lubrication of environmentally compatible lubricants', *Journal of Cleaner Production*, Vol. 373, No. 1, p.133928.

Singh, R. and Sharma, V. (2022) 'Experimental investigations into sustainable machining of Hastelloy C-276 under different lubricating strategies', *Journal of Manufacturing Processes*, Vol. 75, pp.138–153.

Sivalingam, V., Sun, J., Mahalingam, S.K., Nagarajan, L., Natarajan, Y., Salunkhe, S., Nasr, E.A., Davim, J.P. and Hussein, H.M.A.M. (2021) 'Optimization of process parameters for turning Hastelloy X under different machining environments using evolutionary algorithms: a comparative study', *Applied Sciences*, Vol. 11, No. 20, p.9725.

Sun, H., Zou, B., Chen, P., Huang, C., Guo, G., Liu, J., Li, L. and Shi, Z. (2022) 'Effect of MQL condition on cutting performance of high-speed machining of GH4099 with ceramic end mills', *Tribology International*, Vol. 167, No. 1, p.107401.

Talib, N., Sasahara, H. and Rahim, E.A. (2017) 'Evaluation of modified jatropha-based oil with hexagonal boron nitride particle as a biolubricant in orthogonal cutting process', *The International Journal of Advanced Manufacturing Technology*, Vol. 92, No. 1, pp.371–391.

Vasu, V. and Pradeep Kumar Reddy, G. (2011) 'Effect of minimum quantity lubrication with Al_2O_3 nanoparticles on surface roughness, tool wear and temperature dissipation in machining Inconel 600 alloy', *Proceedings of the Institution of Mechanical Engineers, Part N: Journal of Nanoengineering and Nanosystems*, Vol. 225, No. 1, pp.3–16.

Venkatesan, K., Devendiran, S., Sachin, D. and Swaraj, J. (2020. Investigation of machinability characteristics and comparative analysis under different machining conditions for sustainable manufacturing. *Measurement*, *154*, p.107425.

Viswanathan, R., Ramesh, S., Maniraj, S. and Subburam, V. (2020) 'Measurement and multi-response optimization of turning parameters for magnesium alloy using hybrid combination of Taguchi-GRA-PCA technique', *Measurement*, Vol. 159, No. 1, p.107800.

Yıldırım, Ç.V., Sarıkaya, M., Kıvak, T. and Şirin, Ş. (2019) 'The effect of addition of hBN nanoparticles to nanofluid-MQL on tool wear patterns, tool life, roughness and temperature in turning of Ni-based Inconel 625', *Tribology International*, Vol. 134, No. 1, pp.443–456.

Zaman, P.B. and Dhar, N.R. (2020) 'Multi-objective optimization of double-jet MQL system parameters meant for enhancing the turning performance of Ti-6Al-4V alloy', *Arabian Journal for Science and Engineering*, Vol. 45, No. 11, pp.9505–9526.

Zhou, Q., Sivalingam, V., Sun, J., Murugasen, P.K., Gupta, M.K. and Korkmaz, M.E. (2022) 'Understanding the machining induced tribological mechanism of Hastelloy-X under sustainable cooling/lubrication conditions', *The International Journal of Advanced Manufacturing Technology*, Vol. 123, No. 3, pp.973–983.

Appendix

Table A1 ANOVA for machining responses (R_a, F_z, Res)

Responses	*DOF*			*Adjusted sum of square*			*Adjusted mean square*			*F-value*			*P-value*			*Contribution %*		
	R_a	F_z	*Res*	R_a	F_z	*Res*	R_a	F_z	*Res*	R_a	F_z	*Res*	R_a	F_z	*Res*	R_a	F_z	*Res*
V	2	2	2	0.01	12,469	36,721	0.0060	6,234.3	118,361	0.37	13.42	2.27	0.69	0.000	0.132	0.57%	28.43%	9.35 %
f	2	2	2	1.73	14,835	160,179	0.8685	7,417.3	80,090	53.74	15.97	990	0.00	0.000	0.001	81.74%	33.80%	40.77 %
θ	2	2	2	0.05	6,049	44,850	0.0291	3,024.3	22,425	1.80	6.51	2.77	0.19	0.007	0.089	2.74 %	13.87%	11.41 %
L	2	2	2	0.02	2,149	5,484	0.0113	1,074.7	2,742	0.71	2.31	0.34	0.50	0.128	0.717	1.07 %	4.90 %	1.40 %
R – error	18	18	18	0.29	8,363	145,672	0.0161	464.6	8,093							13.72%	19.0 %	37.08 %
Total	26	26	26													100 %	100 %	100 %